Optimized spectral clustering for segmentation of dynamic PET images

Hiba Zbib, Sandrine Mouysset, Simon Stute, Jean-Marc Girault, Jamal Charara, Sylvie Chalon, Laurent Galineau, Irène Buvat, Clovis Tauber

Optimized spectral clustering for segmentation of dynamic PET images

Hiba Zbib* §, Sandrine Mouysset†, Simon Stute‡, Jean-Marc Girault§, Jamal Charara*, Sylvie Chalon§, Laurent Galineau§, Irène Buvat¶ and Clovis Tauber§
*Université Libanaise, Al Hadath, Liban.
§UMRS INSERM U930 - Université de Tours Hopital Bretonneau, France
†CNRS UMR 5055 - Université de Toulouse
‡CEA, Service Hospitalier Frédéric Joliot, France
¶IMNC, Universités Paris 7 & Paris 11, Orsay, France

Email: hibazbib@hotmail.com, clovis.tauber@univ-tours.fr

***Abstract*—The quantification of dynamic PET images requires the definition of regions of interest. The manual delineation is a time consuming and unreproducible process due to the poor resolution of PET images. Approaches were proposed in the literature to classify the kinetic profiles of voxels, however, they are generally either sensitive to initial conditions or favor convex shaped clusters. Recently we have proposed a kinetic spectral clustering (KSC) method for segmentation of dynamic PET images that has the advantage of handling clusters with arbitrary shape in the space in which they are identified. However, its use for clinical applications is still hindered by the manual setting of several parameters. In this paper, we propose an extension of KSC to make it automatic (ASC). A new unsupervised clustering criterion is tailored and a global optimization by a probabilistic metaheuristic algorithm is used to select the scale parameter and the weighting factors involved in the method. We validate our approach with GATE Monte Carlo simulations. Results obtained with ASC compare closely with those obtained with optimal manual parameterization of KSC, and outperform those obtained with two other approaches from the literature.**

I. Introduction

Positron Emission Tomography (PET) is a powerful technique for the in vivo study of physiological and biochemical processes of organs. Such studies require the definition of regions of interest (ROI) to extract the time activity curves (TACs) that are used into compartment models to quantify the target. The definition of regions of interest is generally performed by an expert operator. These manual delineations are a time-consuming, subjective and unreliable process due to noise and poor spatial resolution of PET images. As a result, there is a growing interest in the development of clustering methods that aim at classifying the TAC of voxels in order to separate the PET image into functional regions. Wong et al. [1] proposed to segment dynamic PET images using a Kmeans algorithm, Kim et al. [2] integrated the spatial and temporal information in an hybrid method that uses both cluster analysis and region growing. Maroy et al. [3] estimated the pharmacokinetics far from organ borders and segmented the rodent whole-body PET images by local means analysis followed by hierarchical linkage algorithm to merge regions with similar TAC. Kamasak [4] presented a parametric iterative coordinate descent algorithm for direct nonlinear estimation of kinetic parameters at each voxel from dynamic PET sinogram data. Recently we have proposed a kinetic spectral clustering (KSC) approach for the segmentation of dynamic PET images, which has the advantage of handling arbitrary shaped clusters [5]. It achieved increased precision in the differentiation between functional regions. However it requires manual setting of the parameters involved in the method. In this paper we extend the KSC method by making it automatic (ASC) and therefore more suited for clinical applications. We change the last step of the method to make spectral clustering deterministic, and we combine an original unsupervised clustering criterion and a probabilistic metaheuristic to automatically estimate both the scale parameter of the method and the weighting scheme of the frames of the dynamic PET sequence. In order to validate our approach, GATE Monte Carlo simulations of the Zubal head phantom and a sphere phantom were performed. The ASC was successfully compared with the best result of KSC when the parameters are selected manually and with two other methods from the literature.

II. Proposed method

A. Notations

Let us denote K the number of functional regions supposedly known a priori by the user, T the number of frames contained in the PET image series, N the number of voxels to be clustered and $X_i \in \mathbb{R}^T$ the measured TAC in voxel $i \in [1...N]$.

B. Kinetic spectral clustering for segmentation of dynamic PET images

The KSC of voxel TAC consists in mapping the data into a high dimensional space to increase the separation between clusters, then clustering the data in a reduced space where they are linearly separable [5].

1) Mapping into a high dimensional space: We build the similarity matrix between all pairs of TACs by the calculation of the similarity function S defined as follows:

$$S(X_i, X_j) = \exp(\frac{-d(X_i, X_j)}{2\sigma^2}, \quad (1)$$

where X_i and X_j are the TACs of voxels i and j, σ is a scale parameter that adjusts the distance of patterns mapped into the

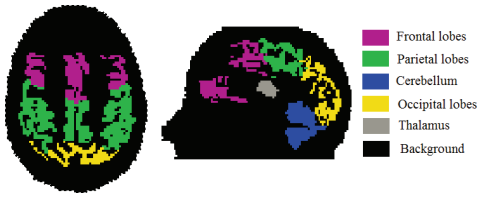

Fig. 1. Regions of the Zubal head phantom used for image simulation.

TABLE I. PARAMETERS USED FOR THE SIMULATION AND THE RECONSTRUCTION OF THE 3 PET SEQUENCES

	Sim.1	Sim.2	Sim.3
Phantom	Sphere	Zubal	Zubal
Medium attenuation	yes	no	yes
Attenuation correction	yes	no	yes
Normalization	yes	no	yes
Iteration numbers	2 iteration	5 iterations	10 iterations
Subset numbers	16 subsets	8 subsets	16 subsets
Noise level	+ +	+	+ + +

feature space, and $d(X_i, X_j)$ is a weighted euclidean distance that we define as:

$$d(X_i, X_j) = (\sum_{l=1}^{T} w_l (X_i(l) - X_j(l))^2)^{1/2} \quad (2)$$

where w_l is the weighting factor of frame l. The noise level in dynamic PET images differs significantly between frames, therefore we include the noise variance in the calculation of the distance between TACs to increase the confidence in frames having less noise. In KSC the weighting factors of each frame were calculated as a noise estimate based on frame duration, time since injection and the number of counts. While this approach allows increased precision in the results, it does not consider the actual activity separation of ROIs. In this paper we propose to consider the weighting factors as parameters of the model and estimate them in a global optimization scheme.

2) Projection into a low dimensional space: We adopt a Laplacian random walk matrix L_{rw} [6]. Spectral clustering using L_{rw} can be interpreted as trying to find a partition of the graph such that the random walk stays long within the same cluster and seldom jumps between clusters. The first K eigenvectors of L_{rw} are calculated, they constitute a new space where the data are projected, which contains the information needed for clustering.

3) Clustering of the projected data: In KSC the projected data are clustered by Kmeans algorithm [5]. Kmeans depends on the initial condition and several runs from different starting centers can be necessary to obtain the best result. To avoid any dependency on initial condition, we propose to use a Global Kmeans approach (GKM) [7] to classify the projected data in the last step of spectral clustering. Compared to KSC, the clustering process of ASC is therefore deterministic, which is a necessary condition for the global optimization of its parameters.

C. Normalized minimal distance

In the segmentation of dynamic PET images two phenomena frequently occur: the separation and the fusion of clusters. To detect these two phenomena, several unsupervised criteria were proposed: Davies and Bouldin [8] proposed an index based on a ratio between the sum of within cluster scatter and between cluster scatter. Dunn [9] proposed a cluster validity index to identify compact and well separated clusters, and defined the diameter of a cluster as the maximal intra cluster distance between all pairs of points. In this paper, we propose a criterion that consists in a robust extension of the Dunn index. We define the normalized minimal distance (NMD) criterion as:

$$NMD = -\frac{\delta_{min}}{\Delta_{max}} \quad (3)$$

where δ_{min} is a minimal inter-cluster distance that decreases when voxels representing similar time courses are assigned to different clusters. It is defined as follows:

$$\delta_{min} = \min_{1 \le o < p \le K} ||C_o - C_p||, \quad (4)$$

where C_o and C_p are the centers of cluster o and p respectively and $||C_o - C_p||$ is the euclidean distance between these two centers. Δ_{max} is a robust maximal intra-cluster distance, that tends to increase when a fusion of clusters occurs. It is defined as:

$$\Delta_{max} = \max_{1 < z < K} \left(\frac{\sum_{i,j \in z} ||X_i - X_j|| A(||X_i - X_j|| \ge dz_{95^{th}})}{N_z \times 0.05}\right), \quad (5)$$

where $dz_{95^{th}}$ is the 95 percentile of intra cluster distances of cluster z, N_z is the number of voxels belonging to z and and A is a Boolean function such that $A(Y) = 1$ if Y is true and 0 otherwise. The proposed NMD criterion increases when a fusion or a splitting of clusters occurs. Compared to the Dunn index which is based on individual points, NMD is less sensitive to outliers and it better represents the quality of clustering for dynamic PET image segmentation.

D. Global optimization of NMD by simulated annealing

We propose to estimate automatically the scale parameter and the weighting factors w_l of each frame by a global optimization scheme using the simulated annealing algorithm [10]. At each iteration the parameter values of ASC are randomly perturbed and the NMD cost function is calculated. Downhill steps are always accepted while uphill steps are accepted to step out of a local minimum under a probability acceptance function that depends on the objective functions and the current temperature.

We bound the search of the scale parameter to the interval between the minimal distance and the 90^{th} percentile of distances between all pairs of TACs. Indeed, in ASC the scale parameter represents a soft threshold of distance between voxels TACs. When σ has a magnitude equivalent to the maximal distance between points, most patterns in the feature space are too close to each other. While when its magnitude is equivalent to the minimal distance, all points are far from every other. We initialize σ by the average distance between every point and its closest neighbor. The bounds of the weighting factors are set as $\forall\ l$, $w_l \in [0\ 1]$, while the initial value for all frames is set to $w_{l0} = 1$.

III. VALIDATION AND EVALUATION

A. Simulation and experimentation

We performed GATE Monte Carlo simulations of Gemini GXL PET 4D acquisitions. A phantom consisting of 12

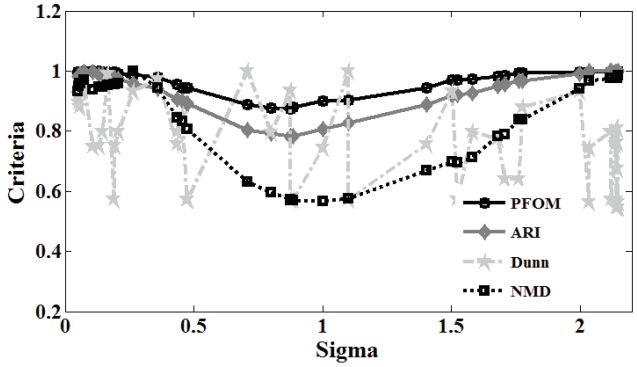

Fig. 2. Comparison between the absolute value of NMD, the Dunn index and the supervised ARI and PFOM criteria (Maximum values of all criteria are normalized to 1).

spheres of different diameters (simulation 1), and the labeled MR image of the Zubal head phantom (simulations 2 and 3) [11] were used as voxelized sources. The regions TAC were generated according to the three-compartment model as proposed by Kamasak et al. [4] and Maroy et al. [3]. We used six regions of the Zubal head phantom for the simulations (figure 1). Each sequence consisted in $5 \times 30s$ followed by $15 \times 60s$ dynamic frames. The reconstruction of dynamic PET images was performed with a fully 3D ANW-OSEM iterative method. In order to assess the quality of segmentation in different conditions of noise level, we used several sets of reconstruction parameters summarized in Table I.

B. Evaluation by supervised criteria

1) Adjusted Rand Index (ARI): Adjusted Rand Index [12] evaluates the consistency between ground truth regions and those of the segmented image. This criterion takes into account the number of pairs of objects grouped into same or different clusters.

2) Pratt's Figure of Merit (PFOM): Pratt's figure of merit measures the precision of edges locations in segmented images, compared to their ground truth location. The PFOM was calculated as follows:

$$PFOM = \frac{1}{max(N_I, N_D)} \sum_{i=1}^{N_D} \frac{1}{1 + \alpha d_i^2} \qquad (6)$$

where N_I and N_D are respectively the number of ideal and detected edge voxels, d_i denotes the distance from the ith-detected edge voxel to the nearest ideal edge voxel and α is a scaling constant set to 1/9 as in Pratt's work [13].

These two supervised criteria lie between 0 and 1. When the segmented results agree perfectly with the ground truth, these criteria are equal to 1.

IV. Results

A. Comparison between the supervised criteria (ARI, PFOM) and the unsupervised criteria (NMD, Dunn index)

We compare our proposed NMD criterion with the Dunn index (to show the improvement that NMD brings in the calculation of the modified intra cluster distance Δ_{max}) and with the supervised criteria ARI and PFOM. The Dunn index and the absolute value of NMD were plotted with the supervised ARI and PFOM criteria versus the values of sigma tested by the simulated annealing (Fig. 2). The Dunn index was more sensitive to noise and outliers, which was predictable as it calculates the intra and inter cluster distances using individual points. NMD criterion was found more robust and representative of cluster distances. As shown in Fig. 2 the Dunn index had more variance compared to other criteria while NMD criterion varied in agreement with the supervised ARI and PFOM criteria. The ARI, PFOM and NMD criteria were found to be associated.

TABLE II. Average and standard deviation of the quantitative criteria.

Phantoms	Criteria	KM	EM	ASC
Simulation 1 Sphere (2it,16sb)	ARI	0.62 ± 0.32	0.20 ± 0.13	0.79 ± 0.20
	PFOM	0.84 ± 0.20	0.49 ± 0.08	0.95 ± 0.04
	NMD	-0.57 ± 0.20	-0.03 ± 0.02	-1.23 ± 0.54
Simulation 2 Zubal (5it,8sb)	ARI	0.73 ±0.13	0.58 ± 0.23	0.86 ± 0.06
	PFOM	0.80 ± 0.11	0.76 ± 0.12	0.93 ± 0.05
	NMD	-0.18 ± 0.09	-0.09 ± 0.09	-0.30 ± 0.10
Simulation 3 Zubal (10it,16sb)	ARI	0.54 ±0.23	0.52 ± 0.22	0.75 ± 0.16
	PFOM	0.73 ± 0.08	0.72 ± 0.11	0.84 ± 0.09
	NMD	-0.15 ± 0.07	-0.08 ± 0.07	-0.19 ± 0.09

B. Comparison of ASC with Kmeans (KM) and Expectation-Maximization (EM) approach

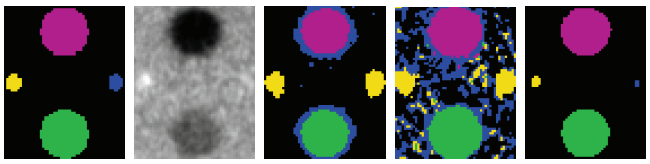

Fig. 3. Axial view of the results obtained for simulation 1: (a) ground truth, (b) one frame from the image series, (c) KM, (d) EM, (e) ASC.

We compared the proposed ASC method with the EM algorithm [14], and the best result that could be obtained with the KM over 100 runs on the 3 simulations.

Figure 3 displays the results for simulation 1. The EM and KM algorithms (Fig. 3(c,d)) correctly detected two big spheres, merged the small spheres and separated the background into two parts. ASC correctly identified all regions (Fig. 3(e)). Two opposite tendencies were observed regarding the small spheres: EM and KM methods tended to overestimate their size while ASC underestimated them. ASC was the only method able to distinguish the two small spheres.

Figure 4 (first row) shows the results for simulation 2, where the level of noise was the lowest of the simulations. The EM algorithm (Fig. 4(d)) merged the occipital lobe with the parietal lobe and several ROI were associated with the background. The KM (Fig. 4(c)) also produced a splitted background while it detected more correctly the regions than EM. However, compared to the ground truth the size of the parietal and occipital lobes were bigger, which was not the

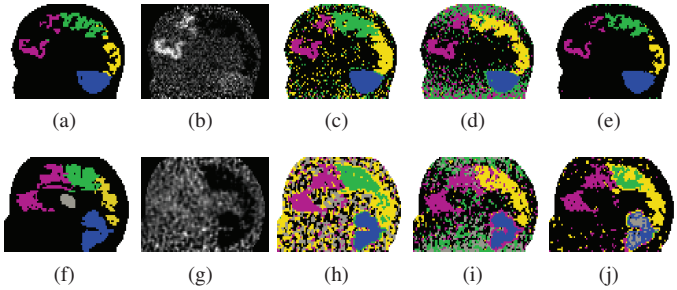

Fig. 4. Sagittal views of the results obtained with the simulations 2 and 3. First row: sagittal view of the results obtained for simulation 2: (a) ground truth,(b) one frame from the image series, (c) KM, (d) EM, (e) ASC. Second row: sagittal view of the results obtained for simulation 3: (f) ground truth, (g) one frame from the image series, (h) KM, (i) EM, (j) ASC.

case with ASC (Fig. 4(e)) where all regions were correctly and more precisely detected.

Figure 4 (second row) shows the results for simulation 3. For this simulation, the attenuation and the normalization were included, and the number of iterations was higher which resulted in high level of noise. The EM and the KM algorithms (Fig. 4(h,i)) did not detect the thalamus and several ROI were merged with the background. With ASC (Fig. 4(j)), the background was less associated with other regions. The parietal, occipital and frontal lobe were correctly detected, but the thalamus was not detected. In this simulation, the 3 methods misclassified some functional regions and especially the thalamus, parietal and occipital lobes. The pixels of the thalamus were very affected by both the noise and the partial volume effect. In ASC the misclassification of the thalamus forced the splitting of another region which corresponded to the cerebellum.

Table II presents the average and the standard deviation of the quantitative criteria ARI, PFOM, and NMD calculated for 8 2D+t slices from the simulation 1, and 20 slices from the simulations 2 and 3 using KM, EM and ASC. ARI, PFOM, and the absolute value of NMD were the smallest for the EM algorithm, while they were the highest for ASC in the 3 simulations. This improvement can be explained by the ability of ASC to separate arbitrary shaped clusters. It also indicates that the global search procedure used to derive the final partition of the data led to acceptable settings of the parameters.

C. Automatic property of ASC

To illustrate the automatic property of ASC, we determined the maximal ARI and PFOM scores that could be obtained with manual selection of parameters of KSC. Then we calculated for 8 2D+t slices from the simulation 1, and for 20 slices from the simulations 2 and 3, the scores of ARI and PFOM obtained with ASC over the maximal scores that could be obtained manually (Table III). The NMD criterion was efficient to select the parameters that gave good segmentation quality of the simulated dynamic PET images, with a percentage of maximal achievable score comprised between 93% and 98%.

TABLE III. PERCENTAGE OF MAXIMAL SCORES OBTAINABLE FROM MANUAL SETTING

	Sim.1	Sim.2	Sim. 3
ARI ASC	93 %	98 %	93 %
PFOM ASC	98 %	97 %	93 %

V. Conclusion

An unsupervised criterion was tailored and optimized by simulated annealing to automatically estimate the input parameters of a spectral clustering method. The ASC results were found very close to the best results obtained with manual selection of the parameters. In addition, ASC was favorably compared with two other approaches: KM and EM. It improved the identifiability of functional regions without a priori knowledge on the kinetic models. The ROI definition offered by ASC and the level of automatization achieved might have significant impact for quantification of dynamic PET images.

Acknowledgment

The authors would like to thank the CNRS in Lebanon and the Lebanese university for supporting this work.

References

[1] K.-P. Wong, D. Feng, S. Meikle, and J. Fulham, "Segmentation of Dynamic PET Images Using Cluster Analysis." *IEEE Trans. NucL. Sci.*, vol. 49, pp. 200–207, 2002.

[2] J. Kim, W. Cai, D. Feng, and S. Eberl, "Segmentation of VOI from Multidimensional Dynamic PET Images by Integrating Spatial and Temporal Features." *IEEE Trans. Inf. Technol. Biomed.*, vol. 10, pp. 637–646, 2006.

[3] R. Maroy, R. Boisgard, C. Comtat, V. Frouin, P. Cathier, E. Duchesnay, F. Dolle, P. E. Nielsen, R. Trebossen, and Tavitian, "Segmentation of Rodent Whole-Body Dynamic PET Images: An Unsupervised Method Based on Voxel Dynamics." *IEEE Trans. Med. Imag.*, vol. 27, pp. 342–354, 2008.

[4] M. E. Kamasak, C. A. Bouman, E. D. Morris, and K. Sauer, "Direct reconstruction of kinetic parameter images from dynamic PET data," *IEEE Trans. Med. Imaging*, vol. 24, pp. 636–650, 2005.

[5] S. Mouysset, H. Zbib, S. Stute, J. Girault, J. Charara, J. Noailles, I. Buvat, and C. Tauber, "Segmentation of dynamic PET images with kinetic spectral clustering," UMRS INSERM U930 Université de Tours, Tech. Rep., 2013.

[6] M. Meila and J. Shi, "A random walks view of spectral segmentation," in *Artificial Intelligence and Statistics*, 2001.

[7] A. Likas, N. Vlassis, and J. J. Verbeek, "The global K-means clustering algorithm," *Pattern Recognition*, vol. 36, pp. 451–461, 2003.

[8] D. Davies and D. W. Bouldin, "A cluster separation measure," *IEEE Trans. Pattern Anal. Mach. Intell.*, vol. 1, pp. 224–227, 1979.

[9] J. C. Dunn, "A fuzzy relative of the isodata process and its use in the detecting compact well-separated clusters," *Journal of Cybernetics*, vol. 3, pp. 32–57, 1973.

[10] S. Kirkpatrick, C. D. Gelett, and M. Vecchi, "Optimization by simulated annealing," *Science*, vol. 220, pp. 671–680, 1983.

[11] I. Zubal, C. R. Harrell, E. O. Smith, Z. Rattner, G. Gindi, and P. B. Hoffer, "Computerized three-dimentional segmented human anatomy," *Med. Phys*, vol. 21, pp. 299–302, 1994.

[12] W. M. Rand, "Objective criteria for the evaluation of clustering method," *Journal of the American Statistical Association*, vol. 66, pp. 846–850, 1971.

[13] W. Pratt, *Digital Image Processing*. Wiley, 1977.

[14] J. Ashburner, J. Haslam, C. Taylor, V. Cunningham, and T. Jones, "A cluster analysis for the characterisation of dynamic PET data." in *Quantification of brain fonction using PET*. San Diego, CA: Academic Press, 1996, ch. 59, pp. 301–306.